JACS
JOURNAL OF THE AMERICAN CHEMICAL SOCIETY
Article
pubs.acs.org/JACS

Poly(isophthalic acid)(ethylene oxide) as a Macromolecular Modulator for Metal–Organic Polyhedra

Teng-Hao Chen,[†] Le Wang,[†] Jonathan V. Trueblood,[†] Vicki H. Grassian,[†,‡] and Seth M. Cohen*[,†]

[†]Department of Chemistry and Biochemistry, University of California, San Diego, La Jolla, California 92093, United States
[‡]Department of Nanoengineering and Scripps Institution of Oceanography, University of California, San Diego, La Jolla, California 92093, United States

Supporting Information

ABSTRACT: A new strategy was developed by using a polymer ligand, poly(isophthalic acid)(ethylene oxide), to modulate the growth of metal–organic polyhedra (MOP) crystals. This macromolecular modulator can effectively control the crystal habit of several different $Cu_{24}L_{24}$ (L = isophthalic acid derivatives) MOPs. The polymer also directed the formation of MOP structures under reaction conditions that only produce metal–organic frameworks in the absence of modulator. Moreover, the polymer also enabled the deposition of MOP crystals on glass surfaces. This macromolecular modulator strategy provides an innovative approach to control the morphology and assembly of MOP particles.

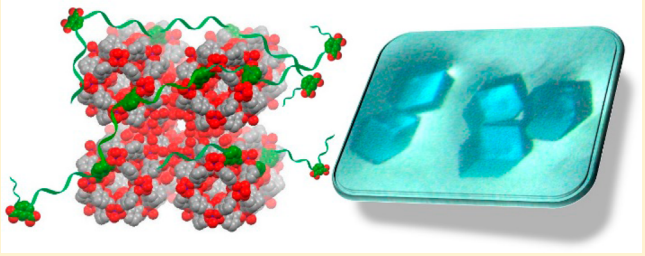

INTRODUCTION

The design and applications of supramolecular architectures based on self-assembly of metal ions and organic building blocks have attracted considerable attention.[1] Supramolecular nanocages are potentially useful for a variety of applications such as selective guest inclusion, gas storage, catalysts, drug delivery, sensing, and nanoscale reaction vessels.[2−8] Metal–organic polyhedra (MOPs) are discrete metal–organic molecular assemblies that feature tailorable internal cavities, rigid molecular structures, and rich chemical functionality.[9−12] Zero-dimensional MOPs can be converted to one-, two-, and three-dimensional architectures via covalent ligand-to-ligand cross-linking,[13,14] and solvent- or coordination-driven assembly.[15−17] Recently, several research groups have connected metal–organic cages by polyethylene glycol (PEG) chains to form new types of hydrogel polymers.[18−20]

Due to their solution processability and uniform accessible cavities, MOPs have been integrated with various kinds of polymers to form mixed-matrix membranes (MMMs) with distinct molecular separation properties.[21−24] In addition to composite materials, organizing porous molecules on surfaces is important for their use in device fabrication for gas adsorption,[25] sensors,[26] catalysts,[27,28] and ionic channels.[29] Despite the developments of porous materials with 3D networks on substrates, bottom-up approaches for organizing MOP crystals and films with specific morphologies, distributions, and arrangements are still lacking. In one example, a hydroxylated MOP could be assembled onto glass surfaces.[30] Other reports described MOPs confined inside lipid bilayers,[29] silica mesopores,[27] and metal–organic frameworks (MOFs)[28] or on plasmonic substrates.[26] These reports rely mostly on soluble MOP molecules that can be solution processed. However, not all MOPs reported exhibit good solubility in common organic solvents.[31] In addition, it would be advantageous to develop a strategy to organize MOP materials in an in situ, one-pot reaction.

The assembly and morphology control of porous materials is crucial for their use in applications and devices.[32] For instance, to optimize the performance of MMMs, control over the size and morphology of fillers is required to minimize the interfacial defects and enhance adhesion between filler and polymer.[33] Polymers such as PEG and polyvinylpyrrolidone (PVP) have been applied to control the growth and morphology of inorganic nanoparticles[34,35] and metal–organic frameworks (MOFs),[36] respectively, via the "oriented attachment" mechanism.[37−39] Unlike MOFs, which are infinite porous networks connected by metal–ligand coordination, MOPs crystallize by the close-packing of discrete cage-like molecules, analogous to small molecule crystallization, which poses different challenges with respect to controlling crystal assembly. To the best of our knowledge, no strategies have been reported to control the growth and morphology of MOP crystals. An efficient method to control the morphology of MOP crystals is therefore needed for the device fabrication such as thin film formation[40] and patterning.[41]

Herein, we report a metal-coordinating polymer (i.e., polymer ligand) that can act as a modulator for controlling the morphology and assembly of MOP crystals. This approach was derived from our recent discovery on polymer metal–organic frameworks (polyMOFs), which employed terephthalic acid derivative polymers as building blocks for MOF syn-

Received: May 20, 2016
Published: July 12, 2016

DOI: 10.1021/jacs.6b04971
J. Am. Chem. Soc. 2016, 138, 9646−9654

thesis.[42,43] Unlike most polymer metal−organic cage (polyMOC) materials using metal-binding groups as the end groups of polymer chains,[18,19,44] the polymer modulator in this work is constructed from 1,3-benzenedicarboxylic acid derivatives (e.g., isophthalic acid, H_2m-bdc) linked by ethylene oxide spacers, where the isophthalic acid component is part of the polymer backbone and recapitulates the building block of the MOP (Figure 1). The poly(isophthalic acid)(ethylene oxide) polymer

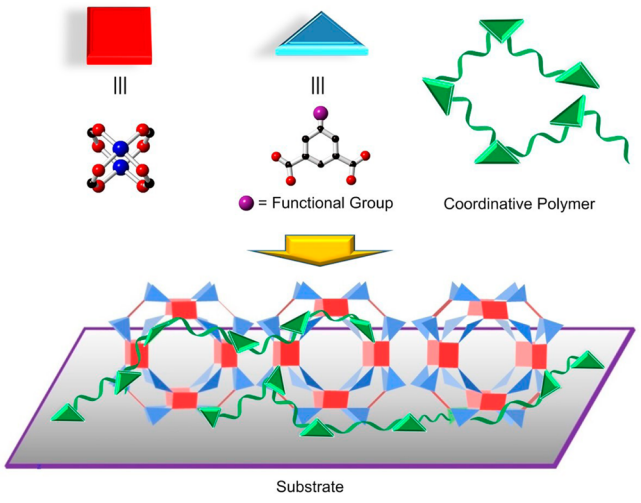

Figure 1. Proposed strategy to use a metal-binding polymer (i.e., polymer ligand) as a modulator for the controlled growth and assembly of MOPs.

1 (Chart 1) not only can coordinate to metal ions, but also results in the growth of crystals with uniform size and morphology in the micrometer size regime. In contrast to polyMOFs and polyMOCs, this polymer does not serve as main building blocks for the resultant porous materials. Control experiments demonstrate that both the coordinating ability of the isophthalic acid and the ethylene oxide linkages are required to elicit this templating effect. In addition, the polymer can be used to support a film of MOP crystals on the surface of glass. This work provides insight into a promising, new route to control the growth and assembly of these metal−organic supramolecular cages.

Chart 1. Polymers and Control Compounds Synthesized in This Work for Study as Coordinating Modulators

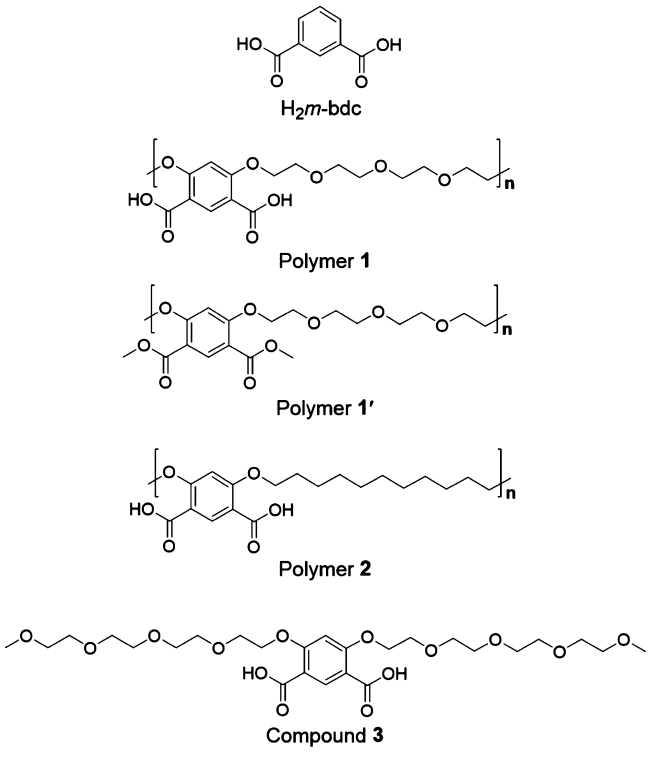

EXPERIMENTAL SECTION

General Information. Starting materials and solvents were purchased and used without further purification from commercial suppliers (Sigma-Aldrich, Alfa Aesar, EMD, TCI, and others). Chromatography was performed using a CombiFlash Rf200 automated system from TeledyneISCO (Lincoln, USA). ^{1}H and ^{13}C nuclear magnetic resonance (NMR) spectra were collected on Varian Mercury spectrometers running at 400 and 500 MHz, respectively. Chemical shifts were quoted in parts per million (ppm) referenced to the appropriate solvent peak. Electrospray ionization mass spectrometry (ESI-MS) was performed at the Molecular Mass Spectrometry Facility (MMSF) in the Department of Chemistry & Biochemistry at the University of California, San Diego. Fourier transform infrared spectroscopy (FT-IR) was performed on a Bruker ALPHA FT-IR spectrometer.

Gel Permeation Chromatography. Gel permeation chromatography (GPC) measurements were performed at 40 °C using an Agilent 1260 Infinity Series liquid chromatography system with an internal differential refractive index detector, and two Waters Styragel HR-5E columns (7.8 mm i.d., 300 mm length, guard column 7.8 mm i.d., 25 mm length). A solution of 0.1% potassium triflate (KOTf) in HPLC grade hexafluoroisopropanol (HFIP) was used as the mobile phase at a flow rate of 0.5 mL/min. Calibration was performed using narrow polydispersity poly(methyl methacrylate) (PMMA) standards. Next, 4.0−6.0 mg of polymer was dissolved in 2.0 mL of HFIP for 1 h. The solution was then filtered through 1 μm membrane before being injected into the GPC instrument.

Single-Crystal X-ray Diffraction Analysis. Single-crystal X-ray diffraction (SXRD) data were collected on a Bruker Apex diffractometer using Mo Kα (λ = 0.71073 Å) radiation. Metal atoms were found in the Fourier difference map and refined anisotropically. The disordered solvent molecules within the cavities were treated with the "SQUEEZE" protocol in PLATON to account for electron density.[45] The crystal data files for MOP-H, -OH, and -NO_2, and pm-MOP-H, -OH, -NO_2, -CH_3, are -NH_2 are available in CIF format as Supporting Information and were deposited into the Cambridge Crystallographic Data Centre (CCDC) and assigned numbers 1478732−1478739.

Analysis by ^{1}H NMR. MOP, MOF, and pm-MOP samples (~5 mg) were digested with sonication in 500 μL of DMSO-d_6 and 5 μL of 35% DCl in D_2O prior to collecting ^{1}H NMR spectra.

Powder X-ray Diffraction Analysis. MOP, MOF, and pm-MOP samples (~15−30 mg) were isolated by filtration and air-dried (~1 min) before powder X-ray diffraction (PXRD) analysis. PXRD data were collected at ambient temperature on a Bruker D8 Advance diffractometer using a LynxEye detector at 40 kV and 40 mA for Cu Kα (λ = 1.5418 Å), with a scan speed of 0.1 s/step, a step size of 0.02 in 2θ, and a 2θ range of 5−40°.

Confocal Raman Microscopy. A LabRam HR evolution Raman spectrometer (Horiba) equipped with an Olympus BX41 optical microscope with 100× magnification lens was used. Raman spectra were recorded in the range of 100−4000 cm^{-1} using a laser operating at 532 nm. Laser power was reduced to 2.5% from the original operating power of 35 mW. Between three and five exposures for 10−30 s were averaged to obtain the resulting spectra.

Gas Sorption Analysis. All gases used were of 99.999% purity. For all samples, the mother liquor was decanted and the resulting crystals were washed with *N*,*N*-dimethylformamide (3 × 10 mL,

DOI: 10.1021/jacs.6b04971
J. Am. Chem. Soc. 2016, 138, 9646−9654

DMF), EtOH (3 × 10 mL), and CH_2Cl_2 (3 × 10 mL). The crystals were stored in CH_2Cl_2 until needed. About 50−100 mg of MOP, MOF, or pm-MOP sample (soaking in CH_2Cl_2) was transferred to a pre-weighed sample tube and evacuated on a vacuum line for 10 min at room temperature. The sample was then degassed at 80 °C on a Micromeritics ASAP 2020 adsorption analyzer for a minimum of 10 h. The sample tube was re-weighed to obtain a consistent mass of the degassed sample. The samples were measured for N_2 (77 and 298 K) and CO_2 (195 and 298 K) adsorption.

RESULTS AND DISCUSSION

Preparation of Compounds 1−3. The H_2*m*-bdc derivative polymers **1** and **2** were prepared by step-growth polymerization (Chart 1, see Supporting Information for details) via Williamson ether synthesis.[42] Dimethyl 4,6-dihydroxy-isophthalate[46] was combined with dibrominated ethylene oxide,[47] 1,11-dibromoundecane, or 2-[2-[2-(2-methoxyethoxy)ethoxy]ethoxy]ethyl bromide to form the ester precursors of **1**-**3**. The hydrolysis of the ester groups afforded polymers **1** and **2**, and a similar synthetic approach was used to produce compound **3**. Both ^{1}H and ^{13}C NMR analysis verified the composition of all compounds (Figures S1−S5). The molecular weight values of polymers **1**, **1′** (the methyl ester precursor of **1**, Chart 1), and **2** were determined by gel permeation chromatography (GPC, Figure S6). The number-average molecular weight (M_n) and weight-average molecular weight (M_w) respectively were 9667 and 17 756 Da for polymer **1**, 12 200 and 22 243 Da for polymer **1′**, and 4000 and 9900 Da for polymer **2**. The polydispersity index (PDI) values were 1.8, 1.8, and 2.5 for polymers **1**, **1′**, and **2**, and are typical for step-growth polymerization.[42] The average degree of polymerization ($DP = M_n/(FW_{repeat\ unit})$) was 27 for polymer **1**, 31 for polymer **1′**, and 12 for polymer **2**. The lower *DP* of polymer **2** was due to poor solubility of its ester precursor in organic solvents that hindered further step-growth polymerization. In addition to GPC, we also performed matrix-assisted laser desorption/ionization time-of-flight (MALDI-TOF) mass spectroscopy. The low solubility of these polymers in common solvents remained a significant barrier to obtaining MALDI-TOF data. After numerous attempts, a low resolution spectrum for polymer **1′** was obtained using α-cyano-4-hydroxycinnamic acid (HCCA) as the matrix (Figure S7). Although only shorter polymer chains were detected (e.g., 5331.20 g/mol corresponding to ∼14 repeat units), the existence of polymeric structure was confirmed. The observed repeating $\Delta m/z$ numbers were close to 176 and 208 g/mol (Figure S7), which are highly indicative of the repeating ethylene oxide chains and methyl isophthalate components of polymer **1′**, respectively.[48] These MALDI-TOF data provide unambiguous evidence for the polymeric nature of the modulators.

MOP-H and Polymer-1-Modulated MOP-H (pm-MOP-H). MOP-1 (we denoted it as MOP-H afterward for comparison with other substituted MOPs), reported by Yaghi and co-workers, is a prototypical truncated cuboctahedron MOP composed of 24 *m*-bdc and 24 Cu(II) ions.[9] First, 1:1 equiv (0.04 mmol) of $Cu(NO_3)_2{\cdot}2.5H_2O$ and H_2*m*-bdc were dissolved in 0.75 mL DMF/0.25 mL EtOH and heated at 80 °C in an oven for 16 h, affording a mixture of prismatic (majority) and tiny cubic (minority) crystals (Figure 2a; also see Supporting Information). The smaller, cubic crystals (∼5 × 5 × 5 μm^3) were not suitable for SXRD analysis. SXRD of the larger prismatic MOP-H crystal (∼100 × 100 × 20 μm^3) revealed a structure $[Cu_{24}(m\text{-bdc})_{24}(S)_{24}]$ (S = terminal solvent molecule, Figure S8) identical to that previously reported for *a*-MOP-H (*a* = anorthic = triclinic).[9] In the same report, crystals with a close-packed, body-centered cubic cell (*c*-MOP-H $[Cu_{24}(m\text{-bdc})_{24}(H_2O)_{24}]$) were obtained after soaking the as-synthesized *a*-MOP-H crystals in the mother liquor for 3 months (as a result of complete hydration).[9] Therefore, the PXRD pattern of our as-synthesized MOP-H displays an impure phase as a result of incomplete hydration, leading to a mixture of *a*-MOP-H and *c*-MOP-H (Figure 3).

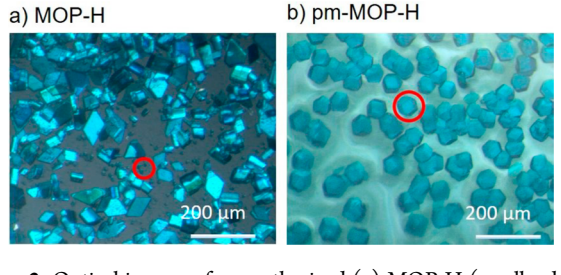

Figure 2. Optical images of as-synthesized (a) MOP-H (small cubic c-MOP-H crystals are circled in red) and (b) pm-MOP-H (large cubic c-MOP-H crystal is circled in red).

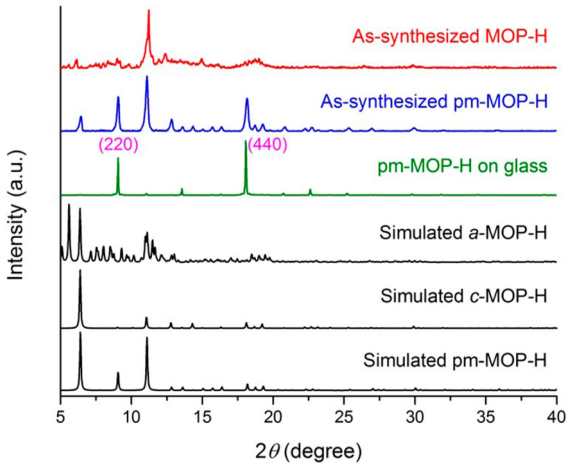

Figure 3. PXRD patterns of materials synthesized from H_2*m*-bdc.

In order to control the morphology of MOP-H crystals, polymer **1** was added as a modulator. Using the same reaction conditions (0.75 mL DMF/0.25 mL EtOH at 80 °C for 16 h) the molar ratio between H_2*m*-bdc and polymer **1** was explored, while keeping the 1:1 molar stoichiometry of $Cu(NO_3)_2{\cdot}2.5H_2O$ to total organic ligands (H_2*m*-bdc and polymer **1**) constant. At a molar ratio 6:1 of H_2*m*-bdc to polymer **1**, the formation of blue crystals with a highly uniform cubic morphology and size were obtained (∼40 × 40 × 40 μm^3, Figure 2b). The morphology of crystals was obviously transformed from prismatic (without modulator) to cubic (with polymer **1** modulator). At other ratios ranging from 2:1 to 20:1 of H_2*m*-bdc to polymer **1**, poorly crystalline solids and mixtures of prismatic and cubic crystals were obtained (Table S1, Figure S9). The structure from a SXRD analysis of the cubic crystals obtained from the 6:1 ratio of H_2*m*-bdc to polymer **1** revealed a close-packing of discrete MOPs ($[Cu_{24}(m\text{-bdc})_{24}(S)_{24}]$), identical to that of *c*-MOP-H (Figure 4a).[9] The PXRD pattern of pm-MOP-H confirmed that a pure phase was obtained with all the characteristic peaks of the simulated pattern from SXRD analysis from pm-MOP-H (Figure 3). After thoroughly washing the isolated crystals with DMF and EtOH,

DOI: 10.1021/jacs.6b04971
J. Am. Chem. Soc. 2016, 138, 9646−9654

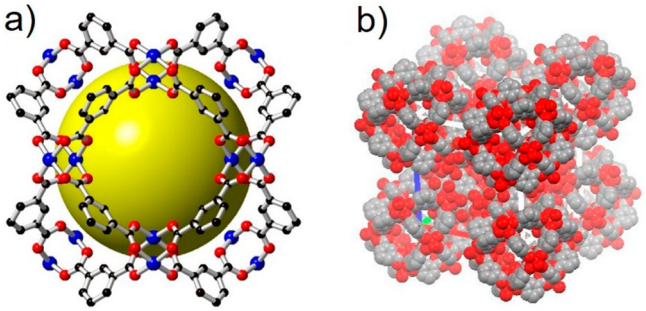

Figure 4. (a) Crystal structure of pm-MOP-H. Cu, blue; O, red; C, black; N, light blue. Terminal solvent molecules (H_2O) and hydrogen atoms have been omitted for clarity. The yellow sphere serves to highlight the void space within the cage. (b) The close-packed cubic unit cell of pm-MOP-H.

the incorporation of polymer **1** was verified by ^{1}H NMR analysis of digested pm-MOP-H in DMSO-d_6 with the addition of a small amount of concentrated DCl/D_2O solution. The NMR analysis indicated that the actual molar ratio of H_2m-bdc to polymer **1** was ~25:1 (Figure S10). Therefore, it is hypothesized that the effective growth and packing of the MOP molecules to form the uniform cubic morphology is largely modulated by polymer **1** at the external crystal surfaces. The hypothesis that the polymer is acting predominantly at the crystal surface is supported by the low amount of polymer associated with the crystals, as well as the close-packing of the *c*-MOP-H nanocages in the crystal lattice, which would appear unable to accommodate the tetra(ethylene oxide) spacers of the polymer (Figure 4b).

As a control reaction, 0.04 mmol of polymer **1** and $Cu(NO_3)_2{\cdot}2.5H_2O$ were combined in a solution of 0.75 mL DMF/0.25 mL EtOH at 80 °C for 16 h. The resulting solid was amorphous as determined by PXRD (Figure S11). Increasing the amount of $Cu(NO_3)_2{\cdot}2.5H_2O$ to 3 equiv under the same reaction conditions resulted in the formation of amorphous materials and CuO (Figure S11). This is consistent with PEG-templating of CuO microstructures, consistent with the templating effect of the ethylene oxide chains of polymer **1**.[49,50]

To examine the role that polymer **1** played in this modulation strategy, we searched for other modulators that might give a similar result. Tetraethylene glycol (TEG), polyethylene glycol with an average molecular weight 400 Da (PEG-400), and polyethylene glycol with average molecular weight of 4000 Da (PEG-4000) were investigated as modulators (Table S1). Keeping the reaction condition unchanged (0.04 mmol of $Cu(NO_3)_2{\cdot}2.5H_2O$ and H_2m-bdc in a solution of 0.75 mL DMF/0.25 mL EtOH at 80 °C for 16 h), the aforementioned PEG polymers were added as modulators. Regardless of length, these PEG polymers without *m*-bdc groups all gave similar results. From the microscopic images, these polymers increased the abundance of cubic crystals compared to the product of modulator-free MOP-H synthesis (Figure S12), but these PEG-only polymers still exhibited a complex mixture of prismatic and cubic crystals, which was confirmed by PXRD analysis (Figure S13). The size of the cubic crystals with PEG-only modulators did increase slightly (about 2-fold, ~10 × 10 × 10 μm^3). However, despite exploring a wide variety of polymer concentrations (Figure S12), the PEG polymers were unable to provide the high degree of uniform control and large crystal size enhancement observed with polymer **1** (compare Figure 2b and Figure S12). Among these ethylene oxide-based additives (polymer **1**, TEG, PEG-400, and PEG-4000), only polymer **1** was able to exclusively produce crystals with uniform size and cubic morphology. This suggests that coordination of polymer **1** to the MOP-H molecules is essential for modulation. Other modulators and additives such as polyvinylpyrrolidone, 4,4′-trimethylenedipiperidine, and tetramethylammonium nitrate[36] were also unable to control the size and morphology of MOP-H crystals (Table S1).

We also synthesized polymer **1′**, polymer **2**, and compound **3** (Chart 1) as modulators for control experiments. Under the same reaction conditions, molar ratios of 3:1, 6:1, and 10:1 of H_2m-bdc to additives were explored (Table S1). Use of polymer **1′** as a modulator, which has the metal-binding carboxylate groups blocked as methyl esters, resulted in a mixture of tiny prismatic and cubic crystals (Figure S14). In addition to the impure phase as confirmed by PXRD analysis (Figure S15), the trace of polymer **1′** was not observed in the in the ^{1}H NMR spectra of the digested product (data not shown). Thus, the requirement of carboxylate groups for effective crystal modulation was verified.

Polymer **2** is an analogue of polymer **1** containing a purely alkyl (e.g., all methylene) instead of a PEG spacer. Polymer **2** gave crystals with poor morphology control (Figure S14) and the PXRD analysis revealed an impure phase (Figure S15). Although polymer **2** was incorporated into the MOP crystals, as determined by ^{1}H NMR analysis of digested samples (Figure S16), the poor control of crystal morphology indicate that the PEG linkers in polymer **1** appear essential for the modulation process.

Compound **3** was prepared as a model of the monomer repeat unit of polymer **1**. Use of compound **3** as a modulator resulted in a mixture of prismatic and cubic crystals (Figure S14) and a mixed phase was confirmed by PXRD analysis (Figure S15). Importantly, compound **3** was not found in the ^{1}H NMR spectra of the digested MOP product (data not shown). Taken together, these control experiments suggested that each feature of polymer **1** is critical for MOP modulation—the combination of H_2m-bdc and ethylene oxide together in a single polymer was crucial for size and morphology control of pm-MOP-H.

pm-MOPs from 5-Substituted H_2m-bdc Derivatives. The successful control of the morphology of pm-MOP-H crystals was generalized with other MOPs. Formation of MOPs with H_2m-bdc derivatives 5-hydroxyisophthalic acid (5-OH-H_2m-bdc), 5-nitroisophthalic acid (5-NO_2-H_2m-bdc), 5-methylisophthalic acid (5-CH_3-H_2m-bdc), and 5-aminoisophthalic acid (5-NH_2-H_2m-bdc) were investigated with polymer **1**. The molar ratio of these H_2m-bdc derivatives to polymer **1** was set to 10:1 for the synthesis of these pm-MOPs. For all pm-MOP samples described below, the ^{1}H NMR spectra of the digested pm-MOPs confirmed that between a 16:1 to 25:1 molar ratio of derivatized *m*-bdc ligand to polymer **1** was incorporated into these crystals (Figure S17). Control experiments carried out under the same reaction conditions without adding modulator or with other additives (e.g., PEG-4000) were also performed, but these other polymers did not exhibit a modulatory affect (see Supporting Information).

MOP-OH and pm-MOP-OH were synthesized in a solution of *N*,*N*-diethylformamide (DEF) and MeOH at 80 °C for 16 h. The MOP-OH crystals formed truncated octahedra with non-uniform sizes (Figure S18). In contrast, pm-MOP-OH presented octahedral blue crystals of highly uniform size

DOI: 10.1021/jacs.6b04971
J. Am. Chem. Soc. 2016, 138, 9646−9654

(~30 × 30 × 30 μm^3, Figure S18). As expected, the SXRD structure determination showed that MOP-OH and pm-MOP-OH possessed the same nanocage structure as that of MOP-H (Figures S19 and S20). PXRD analysis verified the phase purity of MOP-OH and pm-MOP-OH (Figure S21). With pm-MOP-OH, polymer **1** served to produce crystals of a highly uniform size distribution.

Both MOP-NO_2 and pm-MOP-NO_2 crystallized from a solution of DMF and MeOH at 60 °C after 2 d, and both displayed a prismatic crystal morphology (~20 × 20 × 10 μm^3, Figure S22). Their SXRD structures showed the same cage structure as MOP-H (Figures S23 and S24). The phase purity of these materials was confirmed by their PXRD patterns (Figure S21).

Use of 5-CH_3-H_2*m*-bdc in a solution of DMF and MeOH at 60 °C for 2 d without modulator produced tiny crystallites (Figure S25) and PXRD (Figure S21) indicated these crystals consisted of a reported MOF $[Cu(5\text{-}CH_3\text{-}m\text{-}bdc)(H_2O)]_n$,[51] which we denote here as MOF-CH_3-*m*-bdc (Figure S26). Under the same reaction conditions, but with polymer **1** as a modulator, blue prismatic crystals were obtained of uniform size (~20 × 20 × 10 μm^3, Figure S25). The SXRD structure determination of pm-MOP-CH_3 showed the same cage structure as that of MOP-H (Figure S27) with a composition of $[Cu_{24}(5\text{-}CH_3\text{-}m\text{-}bdc)_{24}(S)_{24}]$ (S = solvent). The PXRD pattern of pm-MOP-CH_3 matched that simulated from the SXRD structure (Figure S21), indicating phase purity. Importantly, no example of a MOP has been reported using 5-CH_3-H_2*m*-bdc, as only MOFs have been obtained from this ligand, demonstrating that polymer **1** is modulating and directing not only the crystal habit, but also the formation of a MOP over that of a MOF.

Without polymer **1**, the products synthesized from 5-NH_2-H_2*m*-bdc, from a solution of DMF and MeOH at 60 °C for 2 d, were tiny crystallites (Figure 5a) with PXRD patterns (Figure 6) consistent with a previously reported MOF, $[Cu(5\text{-}NH_2\text{-}m\text{-}bdc)(DMF)]_n$[52] (denoted here as MOF-NH_2-*m*-bdc, Figure S28). In the presence of polymer **1**, under the same reaction condition, uniform green octahedral crystals were obtained of pm-MOP-NH_2 (~30 × 30 × 30 μm^3, Figure 5b). The compound obtained resembles a MOP previously reported by Yaghi and co-workers (MOF-15) that also contained the 5-NH_2-*m*-bdc ligand and Cu(II). The crystal structure of MOP-15 was composed of close-packed $[Cu_{24}(5\text{-}NH_2\text{-}m\text{-}bdc)_{24}(S)_{24}]$ cages.[53] The single crystal structure of pm-MOP-NH_2 $[Cu_{24}(5\text{-}NH_2\text{-}m\text{-}bdc)_{24}(S)_{24}][Cu_{0.5}(S')(S'')]_8$ (where S, S′, S″ represent unspecified solvent molecules) possesses the same MOP cages, but with the MOP molecules connected via an octahedral $Cu(R\text{-}NH_2)_2(S')_2(S'')_2$ center (Figure 7).[54] Each MOP molecule uses 8 amino groups to coordinate to 8 different Cu(II) ions to form a 3-dimensional infinite network. The phase purity of the bulk material was confirmed by PXRD analysis (Figure 6). Taken together, polymer 1 was able to drive the formation of pm-MOP-CH_3 and pm-MOP-NH_2, toward the formation of MOP structures under conditions that normally favor the formation of MOFs.

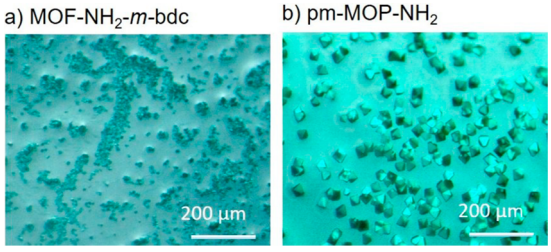

Figure 5. Optical images of as-synthesized (a) MOF-NH_2-*m*-bdc and (b) pm-MOP-NH_2.

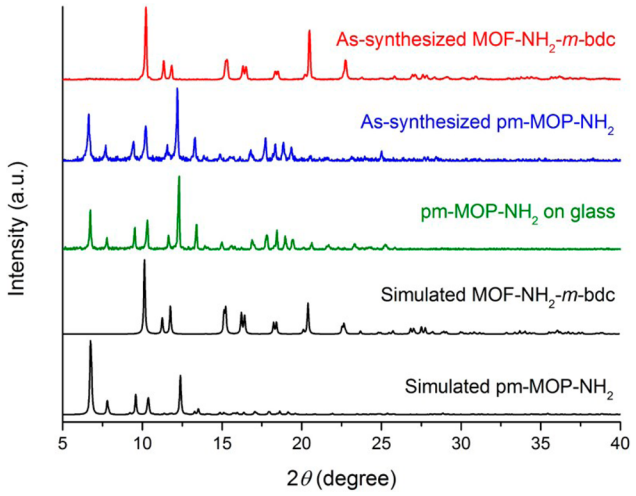

Figure 6. PXRD patterns of materials synthesized from 5-NH_2-H_2*m*-bdc.

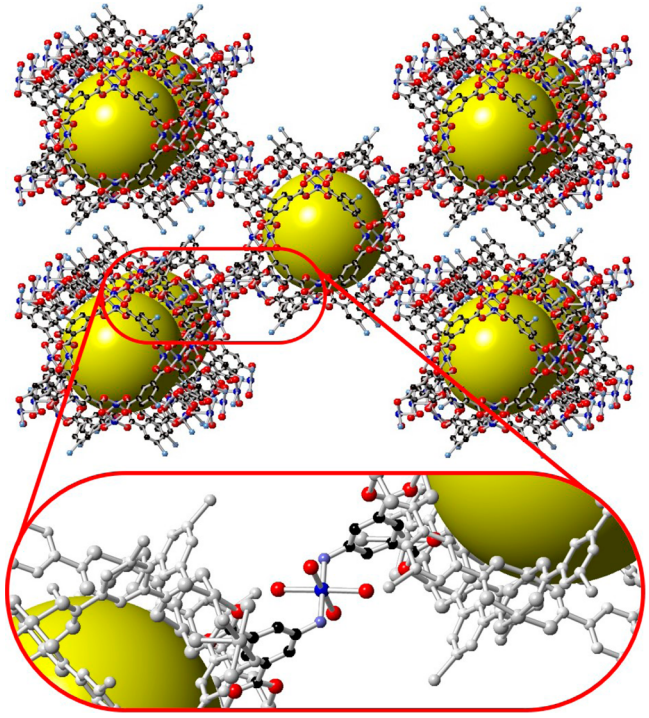

Figure 7. Crystal structure of pm-MOP-NH_2. The red circle highlights the octahedral copper cluster $[Cu(R\text{-}NH_2)_2(S')_2(S'')_2]$ (R = *m*-bdc, S′, S″ = unspecified solvent molecules) that connects the MOP molecules in the crystal structure of pm-MOP-NH_2. Cu, blue; O, red; C, black; N, light blue. Terminal H_2O molecules and hydrogen atoms have been omitted for clarity. The yellow spheres serve to highlight the void space within the cage.

Confocal Raman Microscopy. In order to assess the location of polymer **1** in these materials, confocal Raman microscopy experiments were performed. With the low refractive index of porous materials,[55] this technique can

DOI: 10.1021/jacs.6b04971
J. Am. Chem. Soc. 2016, 138, 9646−9654

analyze the surface of crystals with ~0.2 μm depth resolution.[56] PEG polymers have been characterized by Raman spectroscopy,[57] and several characteristic spectral features of the ethylene oxide chains have been reported.[58] However, polymer **1** showed evidence of fluorescence (Figure 8) upon excitation

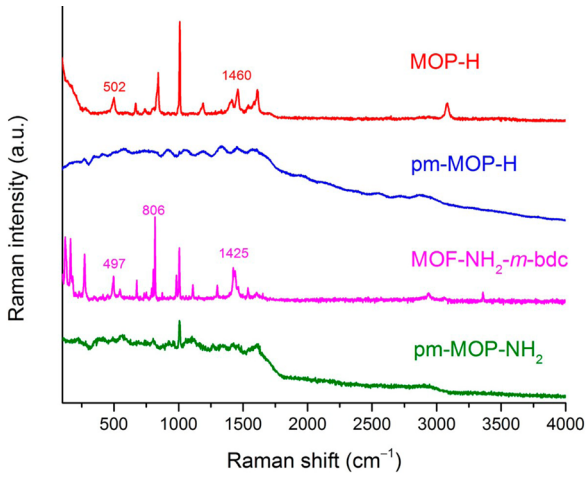

Figure 8. Raman spectra of MOP-H, pm-MOP-H, MOF-NH_2-*m*-bdc, and pm-MOP-NH_2.

in the Raman experiments, perhaps due to the close proximity of isophthalic acid groups in the polymer backbone. The resulting Raman spectra were broad with poor signal-to-noise, which precluded any meaningful peak assignments (Figure S29).

MOPs and MOFs grown in the absence of polymer **1** (e.g., unmodulated crystal growth, MOP-H, -OH, -NO_2, and MOF-CH_3-*m*-bdc, -NH_2-*m*-bdc) all displayed sharp, characteristic Raman spectra that could be assigned based on literature assignments (Figures 8 and S30). For example, Cu−O vibrations (~500 cm^{-1}) and COO symmetric stretching (1415−1460 cm^{-1}) of copper paddlewheel clusters were observed in those spectra (Figures 8 and S30),[59,60] among other characteristic features (Figure S30).[61] In contrast, Raman spectra for all modulated pm-MOPs exhibited a broad, unresolved Raman spectrum resembling that of polymer **1**. These findings suggest that the polymer may not be integrated throughout the crystal but that the Raman laser is going through a polymer film on the surface of the crystal giving rise to the broad unresolved spectrum (Figures 8 and S30). This is consistent with our hypothesis that in these systems the modulator primarily acts and remains at the crystal surfaces.

Presuming polymer **1** is confined to the crystal surfaces, this provides some insight into how crystal modulation is achieved. It is known that poly(ethylene oxide)-based nonionic surfactants can be employed in the templated assembly of hybrid organic−inorganic composites.[37−39] Unlike purely alkane systems (e.g., polymer **2**), ethylene oxide chains can coordinate to transition metal cations,[62] helping to stabilize and facilitate the association of metal-based assemblies, such as MOPs. In the modulation observed here, the ethylene-oxide chains can rapidly coordinate Cu(II) cations, that may then migrate to the carboxylic acid groups in the polymer backbone, which will exhibit stronger binding to Cu(II)[63] and which then possess the correct geometry to initiate formation of MOPs. Subsequently, the large excess of free *m*-bdc ligands can cooperate with, but then ultimately displace the *m*-bdc group of polymer **1** to form a complete MOP. Entropically, the "budding off" of MOPs from polymer **1** would be favored, thus leaving polymer **1** available to template additional MOP particles. Ultimately, the connected chains of coordinating polymer **1** can also serve to constrain packing geometry of MOP molecules forming from the polymer or to which the polymer remains coordinated. This could lead to the observed MOP crystals of uniform morphology and size.

Deposition of pm-MOPs on Glass. Immobilization of MOPs on surfaces has been largely achieved in two steps: synthesis and isolation of soluble MOPs, followed by the slow evaporation of the MOP-containing solution directly onto a substrate.[30,41] During the course of our experiments, it became apparent that pm-MOP crystals tended to adhere to the surface of the glass scintillation vials. It was hypothesized that polymer **1** could mediate the adhesion of pm-MOP crystals onto glass substrates. Thus, by including small pieces of glass (~0.75 × 0.75 cm^2) in the reaction vial, pm-MOPs affixed to glass could be readily isolated. Moreover, making the reaction mixture somewhat more concentrated, a dense packing of pm-MOP crystals could be formed on the glass slides (Table S2). For example, pm-MOP-H was synthesized by heating a solution containing 0.04 mmol of $Cu(NO_3)_2{\cdot}2.5H_2O$, 0.035 mmol of H_2*m*-bdc, and 0.006 mmol of polymer **1** in 0.75 mL DMF/0.25 mL EtOH at 80 °C for 16 h. To form films of pm-MOP-H on glass a solution containing 0.04 mmol of $Cu(NO_3)_2{\cdot}2.5H_2O$, 0.035 mmol of H_2*m*-bdc, and 0.006 mmol of polymer **1** in 0.56 mL DMF/0.19 mL EtOH at 80 °C for 16 h was required. Due to the aggregation/film formation, the crystals comprising these films were small and their morphology could not be clearly observed under optical microscope (unlike the modulated pm-MOPs described above). The deposition of pm-MOP-H, -OH, -NO_2, -CH_3, and -NH_2 was achieved on glass under solvothermal conditions, resulting in a thin layer of crystals (Figures 9, S18, S22, and S25). The identities of these

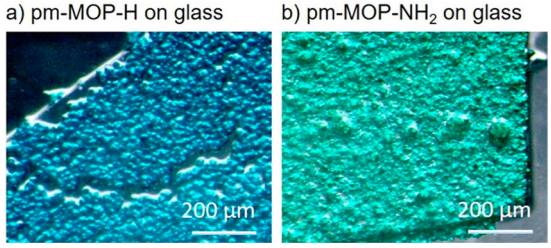

Figure 9. Optical images of as-synthesized (a) pm-MOP-H and (b) pm-MOP-NH_2 deposited on the surface of glass.

deposited pm-MOPs were confirmed by their PXRD patterns (Figures 3, 6, and S21). These films were firmly attached to the glass surface while gently washing with the supernatant solution, but could be easily removed by mechanical stress (e.g., scratching the film surface).

Interestingly, the PXRD pattern of deposited pm-MOP-H displayed two intense peaks at 2θ = 9.1 and 18.1° (Figure 3). These peaks matches the Miller index plane (hkl) = (220) and (440) of a cubic unit cell, respectively, parallel with the (110) plane.[64] Thus, in this film, the discrete MOP molecules show a pronounced preference for packing along the direction perpendicular to the (110) plane of the cubic unit cell as shown in Figure 10. Crystals of tetrahedral or heterocuboidal MOPs have been reported to crystallize with a preferred orientation.[6] However, preferred orientation of MOP crystals of

DOI: 10.1021/jacs.6b04971
J. Am. Chem. Soc. 2016, 138, 9646−9654

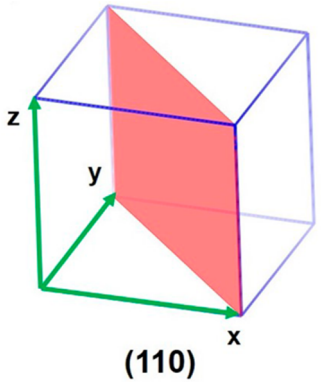

Figure 10. Schematic presentation of Miller index plane (110), which is perpendicular to the preferential growing direction of pm-MOP-H crystals deposited on the surface of glass.

the common truncated cuboctahedral $Cu_{24}L_{24}$ MOPs, as reported here, has never been observed.[65] Among pm-MOPs studied here, preferred orientation was only observed for pm-MOP-H; the PXRD patterns of deposited pm-MOP-NH_2, -OH, -NO_2, and -CH_3 did not display features indicative of preferred orientation (Figures 6 and S21). It may be that the functional groups on the *m*-bdc ligands of these pm-MOPs have a greater effect on the packing of the MOP cages, which prevents the ability of polymer **1** to induce preferred orientation in the films.

Control experiments showed that only MOP-NO_2 and MOF-CH_3-*m*-bdc could be deposited on the surface of glass as a thin layer of crystals without the aid of polymer **1** (Table S2). For the other substituted MOP molecules (-H, -OH, -NH_2) polymer **1** was essential for the deposition of MOP films on the surface of glass using a one-pot solvothermal reaction. Use of other polymers, such as PEG-4000 had no apparent affect and did not result in the formation of films (Table S3, Figure S31). Overall, polymer **1** possessed the unique ability to effectively confine discrete MOP molecules with various functional groups onto the surface of glass using one-pot solvothermal conditions, providing a general route to the processing of these metal–organic cage materials.

Gas Sorption Studies. N_2 (77 and 298 K) and CO_2 (195 and 298 K) gas sorption studies were performed on all porous materials synthesized in this work. After solvent exchange with EtOH and CH_2Cl_2 for 3 d, all MOP, MOF, and pm-MOP samples were activated at 80 °C for 10 h in order to activate the samples for gas sorption analysis. Because the crystals of MOPs and pm-MOPs were composed of close-packed discrete MOP molecules, removing solvent from the crystals results in loss of bulk crystallinity as confirmed by PXRD analysis (data not shown), but the intrinsic porosities of these MOPs are retained. Generally, at 298 K and 1 atm, all MOPs and pm-MOPs displayed CO_2 adsorption range from 10 to 35 $cm^3\ g^{-1}$, but negligible N_2 adsorption (Figures 11 and S35). These results are comparable with that of other MOP studies.[31] At low temperature, MOPs and pm-MOPs exhibited very distinct adsorption behaviors. pm-MOP-CH_3 and pm-MOP-NH_2 lacked a modulator-free MOP counterpart (because they form MOFs in the absence of polymer **1**), but behaved similar to other pm-MOPs reported here (Figure S35).

At 77 K and 1 atm, the N_2 adsorptions of MOP-H, -OH, and -NO_2 were 140, 100, and 130 $cm^3\ g^{-1}$, respectively. In contrast, pm-MOPs all displayed negligible N_2 adsorption. The reason

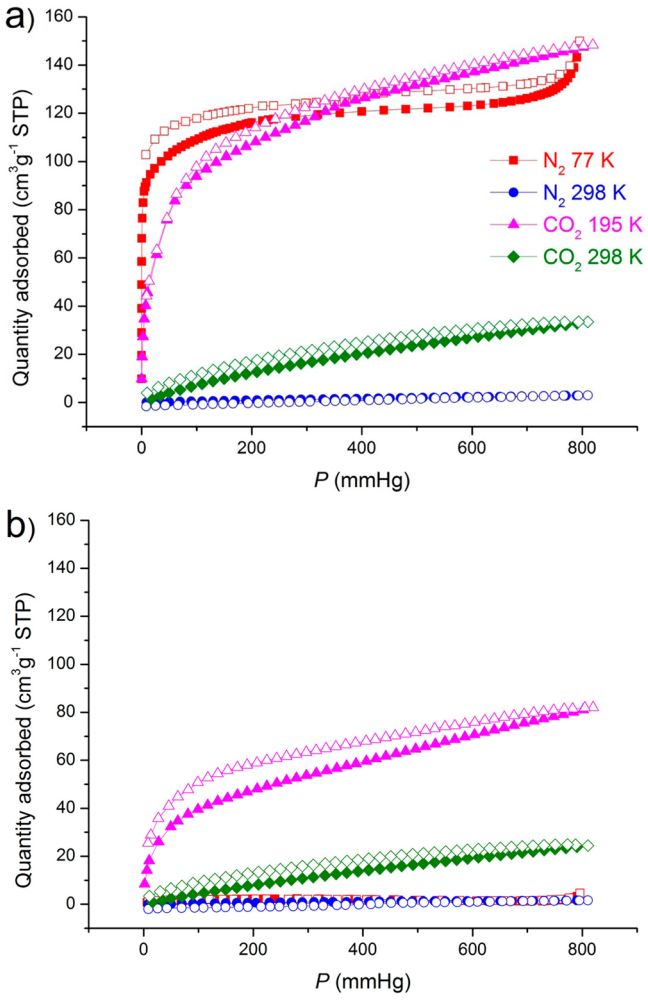

Figure 11. N_2 (77 K, red; 298 K, blue) and CO_2 (195 K, magenta; 298 K, green) sorption isotherms of activated (a) MOP-H and (b) pm-MOP-H. Filled symbols: adsorption; open symbols: desorption.

for this dramatic change may be that if polymer **1** is coordinated to the surface of pm-MOP crystals then the polymer may block the accessible windows for gas uptake. At 195 K and 1 atm, the CO_2 capacities of MOP-H, -OH, and -NO_2 were 140, 100, and 80 $cm^3\ g^{-1}$, while those of pm-MOP-H, -OH, -NO_2, -CH_3, and -NH_2 were 80, 65, 80, 75, and 70 $cm^3\ g^{-1}$ (Figures 11 and S35). The largest difference was between MOP-H and pm-MOP-H (42% reduction, Figure 11). In general, the persistent CO_2 capacity for the pm-MOPs indicates that the cavities are not fully occupied or occluded by polymer **1**.

CONCLUSIONS

In this study, we designed and synthesized a poly(isophthalic acid)(ethylene oxide) polymer **1** and used it as a coordinative modulator for MOP synthesis. This strategy has not been previously reported in MOP chemistry and was shown to be general for a series of substituted MOPs. Several interesting findings were achieved with this polymer modulator. First, the prototypical MOP-H, which normally manifests as two different crystal phases with irregular sized crystals, was reduced to a single, cubic crystal phase with a much larger, uniform crystal size (pm-MOP-H). Similar morphology control was observed for pm-MOP-OH, -NO_2, -CH_3, and -NH_2. Second, the polymer

DOI: 10.1021/jacs.6b04971
J. Am. Chem. Soc. 2016, 138, 9646–9654

modulator was able to divert the synthesis of MOFs in favor of a MOP architecture for pm-MOP-CH_3 and pm-MOP-NH_2. Third, the polymer modulator enabled the formation of robust pm-MOP films on glass, and in one case (pm-MOP-H) a strong preferred orientation was exhibited. Using this approach, we anticipate a variety of polymer ligand modulators can be designed for different MOPs or other supramolecular materials. Achieving efficient morphology and size control of MOP crystals will be of great benefit to the formation of MOP membranes[40] and MMMs that utilize MOP fillers.[66] Thus, this work will help enable MOPs to play a great role in porous materials, membranes, and separations chemistry. Overall, these findings provide a new strategy for modulating the crystal growth and processing of supramolecular nanocages in situ.

■ ASSOCIATED CONTENT

Supporting Information

The Supporting Information is available free of charge on the ACS Publications website at DOI: 10.1021/jacs.6b04971.

Experimental details and additional data, including Figures S1−S35 and Tables S1−S11 (PDF)

X-ray crystallographic data for MOP-H, MOP-OH, MOP-NO_2, pm-MOP-H, pm-MOP-OH, pm-MOP-NO_2, pm-MOP-CH_3, and pm-MOP-NH_2 (CIF)

■ AUTHOR INFORMATION

Corresponding Author

*scohen@ucsd.edu

Notes

The authors declare no competing financial interest.

■ ACKNOWLEDGMENTS

We acknowledge financial support from the U.S. Department of Energy, Office of Basic Energy Sciences, Division of Materials Science and Engineering under Award No. DE-FG02-08ER46519. We thank the Molecular Mass Spectrometry Facility (Dr. Yongxuan Su, UC San Diego) for assistance with mass spectrometry experiments. We thank Ha Thi Hoang Nguyen and Prof. Stephen A. Miller of the University of Florida, Gainsville, for assistance with GPC analysis of polymer samples.

■ REFERENCES

(1) Cook, T. R.; Zheng, Y.-R.; Stang, P. J. *Chem. Rev.* **2013**, *113*, 734.
(2) Lu, W.; Yuan, D.; Yakovenko, A.; Zhou, H.-C. *Chem. Commun.* **2011**, *47*, 4968.
(3) Wang, X.-S.; Ma, S.; Forster, P. M.; Yuan, D.; Eckert, J.; López, J. J.; Murphy, B. J.; Parise, J. B.; Zhou, H.-C. *Angew. Chem., Int. Ed.* **2008**, *47*, 7263.
(4) Zhao, D.; Tan, S.; Yuan, D.; Lu, W.; Rezenom, Y. H.; Jiang, H.; Wang, L.-Q.; Zhou, H.-C. *Adv. Mater.* **2011**, *23*, 90.
(5) Takezawa, H.; Murase, T.; Resnati, G.; Metrangolo, P.; Fujita, M. *J. Am. Chem. Soc.* **2014**, *136*, 1786.
(6) Sudik, A. C.; Millward, A. R.; Ockwig, N. W.; Côté, A. P.; Kim, J.; Yaghi, O. M. *J. Am. Chem. Soc.* **2005**, *127*, 7110.
(7) Jing, X.; He, C.; Yang, Y.; Duan, C. *J. Am. Chem. Soc.* **2015**, *137*, 3967.
(8) Park, J.; Sun, L.-B.; Chen, Y.-P.; Perry, Z.; Zhou, H.-C. *Angew. Chem., Int. Ed.* **2014**, *53*, 5842.
(9) Eddaoudi, M.; Kim, J.; Wachter, J. B.; Chae, H. K.; O'Keeffe, M.; Yaghi, O. M. *J. Am. Chem. Soc.* **2001**, *123*, 4368.
(10) Tranchemontagne, D. J.; Ni, Z.; O'Keeffe, M.; Yaghi, O. M. *Angew. Chem., Int. Ed.* **2008**, *47*, 5136.
(11) Moulton, B.; Lu, J.; Mondal, A.; Zaworotko, M. J. *Chem. Commun.* **2001**, 863.
(12) Li, J.-R.; Zhou, H.-C. *Nat. Chem.* **2010**, *2*, 893.
(13) Perry; Kravtsov, V. C.; McManus, G. J.; Zaworotko, M. J. *J. Am. Chem. Soc.* **2007**, *129*, 10076.
(14) Qiu, W.; Perman, J. A.; Wojtas, L.; Eddaoudi, M.; Zaworotko, M. J. *Chem. Commun.* **2009**, *46*, 8734.
(15) Liu, T.-F.; Chen, Y.-P.; Yakovenko, A. A.; Zhou, H.-C. *J. Am. Chem. Soc.* **2012**, *134*, 17358.
(16) Niu, Z.; Fang, S.; Liu, X.; Ma, J.-G.; Ma, S.; Cheng, P. *J. Am. Chem. Soc.* **2015**, *137*, 14873.
(17) Li, J.-R.; Timmons, D. J.; Zhou, H.-C. *J. Am. Chem. Soc.* **2009**, *131*, 6368.
(18) Foster, J. A.; Parker, R. M.; Belenguer, A. M.; Kishi, N.; Sutton, S.; Abell, C.; Nitschke, J. R. *J. Am. Chem. Soc.* **2015**, *137*, 9722.
(19) Zhukhovitskiy, A. V.; Zhong, M.; Keeler, E. G.; Michaelis, V. K.; Sun, J. E. P.; Hore, M. J. A.; Pochan, D. J.; Griffin, R. G.; Willard, A. P.; Johnson, J. A. *Nat. Chem.* **2016**, *8*, 33.
(20) Kawamoto, K.; Grindy, S. C.; Liu, J.; Holten-Andersen, N.; Johnson, J. A. *ACS Macro Lett.* **2015**, *4*, 458.
(21) Zhao, C.; Wang, N.; Wang, L.; Sheng, S.; Fan, H.; Yang, F.; Ji, S.; Li, J.-R.; Yu, J. *AIChEJ.* **2016**, DOI: 10.1002/aic.15263.
(22) Zhao, C.; Wang, N.; Wang, L.; Huang, H.; Zhang, R.; Yang, F.; Xie, Y.; Ji, S.; Li, J.-R. *Chem. Commun.* **2014**, *50*, 13921.
(23) Perez, E. V.; Balkus, K. J., Jr.; Ferraris, J. P.; Musselman, I. H. *J. Membr. Sci.* **2014**, *463*, 82.
(24) Kitchin, M.; Teo, J.; Konstas, K.; Lau, C. H.; Sumby, C. J.; Thornton, A. W.; Doonan, C. J.; Hill, M. R. *J. Mater. Chem. A* **2015**, *3*, 15241.
(25) Li, J.-R.; Yu, J.; Lu, W.; Sun, L.-B.; Sculley, J.; Balbuena, P. B.; Zhou, H.-C. *Nat. Commun.* **2013**, *4*, 1538.
(26) Wang, C.; Shang, J.; Lan, Y.; Tian, T.; Wang, H.; Chen, X.; Gu, J.-Y.; Liu, J. Z.; Wan, L.-J.; Zhu, W.; Li, G. *Adv. Funct. Mater.* **2015**, *25*, 6009.
(27) Kang, Y.-H.; Liu, X.-D.; Yan, N.; Jiang, Y.; Liu, X.-Q.; Sun, L.-B.; Li, J.-R. *J. Am. Chem. Soc.* **2016**, *138*, 6099.
(28) Qiu, X.; Zhong, W.; Bai, C.; Li, Y. *J. Am. Chem. Soc.* **2016**, *138*, 1138.
(29) Jung, M.; Kim, H.; Baek, K.; Kim, K. *Angew. Chem., Int. Ed.* **2008**, *47*, 5755.
(30) Abourahma, H.; Coleman, A. W.; Moulton, B.; Rather, B.; Shahgaldian, P.; Zaworotko, M. J. *Chem. Commun.* **2001**, 2380.
(31) Ahmad, N.; Chughtai, A. H.; Younus, H. A.; Verpoort, F. *Coord. Chem. Rev.* **2014**, *280*, 1.
(32) Falcaro, P.; Ricco, R.; Doherty, C. M.; Liang, K.; Hill, A. J.; Styles, M. J. *Chem. Soc. Rev.* **2014**, *43*, 5513.
(33) Denny, M. S.; Cohen, S. M. *Angew. Chem., Int. Ed.* **2015**, *54*, 9029.
(34) Shao, S.; Zheng, K.; Pullerits, T.; Zhang, F. *ACS Appl. Mater. Interfaces* **2013**, *5*, 380.
(35) Taubert, A.; Palms, D.; Weiss, Ö.; Piccini, M.-T.; Batchelder, D. N. *Chem. Mater.* **2002**, *14*, 2594.
(36) Pang, M.; Cairns, A. J.; Liu, Y.; Belmabkhout, Y.; Zeng, H. C.; Eddaoudi, M. *J. Am. Chem. Soc.* **2012**, *134*, 13176.
(37) Blin, J.-L.; Léonard, A.; Yuan, Z.-Y.; Gigot, L.; Vantomme, A.; Cheetham, A. K.; Su, B.-L. *Angew. Chem., Int. Ed.* **2003**, *42*, 2872.
(38) Yuan, Z. Y.; Ren, T. Z.; Su, B. L. *Adv. Mater.* **2003**, *15*, 1462.
(39) Yang, H. G.; Zeng, H. C. *Angew. Chem., Int. Ed.* **2004**, *43*, 5206.
(40) Song, Q.; Jiang, S.; Hasell, T.; Liu, M.; Sun, S.; Cheetham, A. K.; Sivaniah, E.; Cooper, A. I. *Adv. Mater.* **2016**, *28*, 2629.
(41) Furukawa, H.; Kim, J.; Plass, K. E.; Yaghi, O. M. *J. Am. Chem. Soc.* **2006**, *128*, 8398.
(42) Zhang, Z.; Nguyen, H. T. H.; Miller, S. A.; Cohen, S. M. *Angew. Chem., Int. Ed.* **2015**, *54*, 6152.
(43) Zhang, Z.; Nguyen, H. T. H.; Miller, S. A.; Ploskonka, A. M.; DeCoste, J. B.; Cohen, S. M. *J. Am. Chem. Soc.* **2016**, *138*, 920.
(44) Hosono, N.; Gochomori, M.; Matsuda, R.; Sato, H.; Kitagawa, S. *J. Am. Chem. Soc.* **2016**, *138*, 6525.
(45) Spek, A. *J. Appl. Crystallogr.* **2003**, *36*, 7.

DOI: 10.1021/jacs.6b04971
J. Am. Chem. Soc. 2016, 138, 9646−9654

(46) Wu, X.; Liang, G.; Ji, G.; Fun, H.-K.; He, L.; Gong, B. *Chem. Commun.* **2012**, *48*, 2228.
(47) Chen, T.-H.; Schneemann, A.; Fischer, R. A.; Cohen, S. M. *Dalton Trans.* **2016**, *45*, 3063.
(48) Marie, A.; Fournier, F.; Tabet, J. C. *Anal. Chem.* **2000**, *72*, 5106.
(49) Wang, W.; Zhou, Q.; Fei, X.; He, Y.; Zhang, P.; Zhang, G.; Peng, L.; Xie, W. *CrystEngComm* **2010**, *12*, 2232.
(50) Wang, W.; Zhan, Y.; Wang, X.; Liu, Y.; Zheng, C.; Wang, G. *Mater. Res. Bull.* **2002**, *37*, 1093.
(51) Zou, R.-Q.; Sakurai, H.; Han, S.; Zhong, R.-Q.; Xu, Q. *J. Am. Chem. Soc.* **2007**, *129*, 8402.
(52) Xiao, H.-P.; Li, X.-H.; Morsali, A.; Wang, J.-G.; Zhang, W.-B. *Z. Anorg. Allg. Chem.* **2007**, *633*, 1107.
(53) Furukawa, H.; Kim, J.; Ockwig, N. W.; O'Keeffe, M.; Yaghi, O. M. *J. Am. Chem. Soc.* **2008**, *130*, 11650.
(54) From SXRD analysis, all MOP crystals were weakly diffracting, and the coordinated disordered solvent molecules could not be conclusively determined. In the case of pm-MOP-NH_2, two pairs of Cu−O bonds with distances 2.16 and 2.42 Å were found in the octahedral copper cluster that connects two distinct MOP molecules. Thus, we assign the corresponding solvent molecules as S′ and S″.
(55) So, M. C.; Beyzavi, M. H.; Sawhney, R.; Shekhah, O.; Eddaoudi, M.; Al-Juaid, S. S.; Hupp, J. T.; Farha, O. K. *Chem. Commun.* **2015**, *51*, 85.
(56) Juang, C. B.; Finzi, L.; Bustamante, C. J. *Rev. Sci. Instrum.* **1988**, *59*, 2399.
(57) Chen, C.; Yao, T.; Tu, S.; Xu, W.; Han, Y.; Zhou, P. *Phys. Chem. Chem. Phys.* **2016**, *18*, 16353.
(58) Machida, K.; Miyazawa, T. *Spectrochim. Acta* **1964**, *20*, 1865.
(59) Prestipino, C.; Regli, L.; Vitillo, J. G.; Bonino, F.; Damin, A.; Lamberti, C.; Zecchina, A.; Solari, P. L.; Kongshaug, K. O.; Bordiga, S. *Chem. Mater.* **2006**, *18*, 1337.
(60) Tan, K.; Nijem, N.; Canepa, P.; Gong, Q.; Li, J.; Thonhauser, T.; Chabal, Y. J. *Chem. Mater.* **2012**, *24*, 3153.
(61) Shlyapochnikov, V. A.; Khaikin, L. S.; Grikina, O. E.; Bock, C. W.; Vilkov, L. V. *J. Mol. Struct.* **1994**, *326*, 1.
(62) Soler-Illia, G. J. d. A. A.; Sanchez, C. *New J. Chem.* **2000**, *24*, 493.
(63) Soler-Illia, G. J. d. A. A.; Scolan, E.; Louis, A.; Albouy, P.-A.; Sanchez, C. *New J. Chem.* **2001**, *25*, 156.
(64) The Miller index of intense peaks was assigned according to the simulated PXRD pattern from the single-crystal structure using the software Mercury 3.5.
(65) Ahmad, N.; Younus, H. A.; Chughtai, A. H.; Verpoort, F. *Chem. Soc. Rev.* **2015**, *44*, 9.
(66) Bushell, A. F.; Budd, P. M.; Attfield, M. P.; Jones, J. T. A.; Hasell, T.; Cooper, A. I.; Bernardo, P.; Bazzarelli, F.; Clarizia, G.; Jansen, J. C. *Angew. Chem., Int. Ed.* **2013**, *52*, 1253.

DOI: 10.1021/jacs.6b04971
J. Am. Chem. Soc. 2016, 138, 9646−9654